DIRECT EFFECTS OF GRAVITY ON CAVITATION BUBBLE COLLAPSE

A. de Bosset[1], D. Obreschkow[1,2], P. Kobel[1,3], N. Dorsaz[1,4], and M. Farhat[1]

[1] *Laboratoire des Machines Hydrauliques, EPFL, 1007 Lausanne, Switzerland*
[2] *Astrophysics, Department of Physics, University of Oxford, Keble Road, Oxford, OX1 3RH, UK*
[3] *Max Planck Institute for Solar System Research, 37191 Katlenburg-Lindau, Germany*
[4] *Institut Romand de Recherche Numérique en Physique des Matériaux, EPFL, 1015 Lausanne, Switzerland*

We propose an experiment for studying the final stages of collapse of a single laser generated cavitation bubble in microgravity. Unlike previous investigations, the goal of the study is to examine the direct effects of gravity on the cavity collapse. In this paper we present ground-based research on these effects and outline a microgravity experiment destined for ESA Microgravity Research Campaign. The proposed experiment uses a focused laser to generate a highly spherical bubble in an extended water volume without disturbing the liquid and measures bubble rebound and shockwave intensity. Buoyancy forces being proportional to bubble volume, smaller bubbles are the least disturbed. Results show that as bubble size decreases, the part of bubble energy transformed into a shockwave increases, to the detriment of the rebound bubble and liquid jets.

Introduction

Cavitation is a major source of erosion in industrial hydraulic machines such as rocket boosters, pumps and water turbines. In such system low pressure regions exist where the water literally rips apart and pockets of water vapour (nearly vacuums) form. These pockets, called "cavitation bubbles" or "cavities", are transported to high pressure regions, where they immediately collapse. At the last stage of this collapse, erosive damage is caused by the emission of liquid jets and shockwaves. While cavitation bubbles typically appear in groups (e.g. behind ship propellers), specific experiments often intend to produce single bubbles to probe the physics behind their evolution, in particular the last stage of their collapse.

During a bubble collapse the initial hydrodynamic bubble energy is redistributed in at least five distinct channels, as illustrated in Figure 1: (1) a new, subsequent bubble caused by a partially elastic rebound, (2) shockwaves, (3) liquid jets, (4) electromagnetic radiation (if visible, the phenomenon is called "sonoluminescence"), (5) thermal motion, and arguably (6) cold nuclear fusion. The rebound bubble distributes its energy in the same channels, when collapsing. The relative amount of energy released in each of these energy channels strongly depends on the sphericity of the collapsing bubble at its very last stage. This sphericity is determined by the presence of boundaries (e.g. a solid surface of a propeller blade or a free water surface) and inertial forces, such as centrifugal forces and gravity.

Illustratively, Benjamin and Ellis (Benjamin and Ellis 1966) demonstrated that large bubbles will deform due to the gravitational pressure field in water (i.e. "buoyancy"), influencing the cavity collapse and causing preferential microjet propagation and an increase of the energy fraction carried by the microjet. First microgravity experiments by (Matula 2000) accordingly suggest that sonoluminescence increases during periods of microgravity. To understand the dependence of the energy distribution on bubble sphericity, it is crucial to study the ideal case of a perfectly spherical bubble. This requires the removal of boundaries close the collapsing bubble and, more importantly, the removal of all inertial forces including gravity – thus the motivation of probing collapsing bubbles in microgravity.
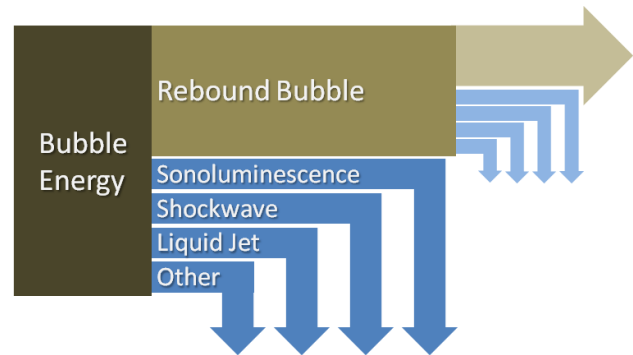

Figure 1 : Energy Flow; Dissipation mechanisms

In this paper we outline a new microgravity experiment destined for ESA Parabolic Flight Campaigns investigating the direct effects of gravity on cavitation bubble collapse. We begin with a summary of the basic theory behind single bubble dynamics. The proposed experiment uses a focused laser to generate a highly spherical bubble in an extended water volume without disturbing the liquid. Considerable effort has been made to minimize all effects, other than gravity, which may disturb bubble sphericity. On parabolic flights, it will be possible to compare many different gravity levels (0g to 1.8g) under otherwise identical conditions. The rapid cavity evolution is recorded using a fast visualization system and shockwaves are detected using micro piezo pressure sensors. Important details concerning the optical setup are included. A design for a novel laser beam expander is discussed and tested. Finally, results from the ground based research carried out with the aforementioned experiment will be presented.

Background

The Rayleigh-Plesset (Rayleigh 1917) & (Plesset 1949) equation describes the evolution of a cavity located in an infinite medium,

$$-\Delta p / \rho = 1.5\dot{R}^2 + R\ddot{R} \qquad (1.1)$$

Where Δp is the pressure difference at the bubble interface, ρ is the density of the surrounding fluid, and R(t) is the bubble radius. This equation holds true if the bubble is placed "far" from a solid surface relative to its diameter, thus avoiding any

disturbance of the collapse process. If the distance to the nearest solid surface is at least five times that of the maximum radius, the bubble is considered in a quasi-infinite medium.

Equation (1.1) can be integrated from the edge of the bubble, i.e. the interface, to infinity. This gives the well known equation (1.2), which links the bubble maximum radius to the Rayleigh collapse time (Rayleigh 1917).

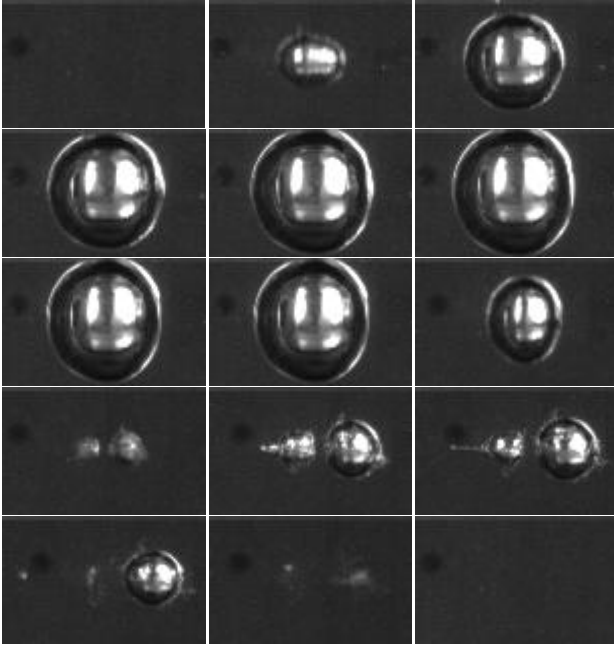$$T_{rayl} = 0.915 R_{max} \sqrt{\rho / \Delta p} \qquad (1.2)$$

Figure 2 : Typical cavity life cycle (20µs between images)

A cavity can be generated experimentally when a large amount of energy is deposited in a small point-like area. A critical energy density must be reached in order for the water to ionize. The hot plasma expands explosively, while cooling adiabatically and recombining into low density water vapour. The cavity thus created has an absolute pressure which is negligible compared to the pressure of the surrounding water. This large difference in pressure causes a subsequent collapse. Figure 2 shows the evolution of a laser generated cavity filmed by the high speed camera of our setup.

The potential energy of the bubble can be calculated given its diameter, and assuming the bubble is filled with water vapour at the saturation pressure, p_v. When the bubble maximum radius is reached (end of growth and beginning of collapse), only the potential energy is left,

$$E_{pot} = \int_0^{R_{max}} 4\pi r^2 \Delta P \cdot dr = \tfrac{4}{3}\pi R_{max}^3 \Delta P \qquad (1.3)$$

Where $\Delta P = p_{atm} - p_v \approx p_{atm} = 10^5 Pa$.

The experiment described in the next paragraph is designed to probe how this energy is distributed between each dissipation channel.

Experimental Setup

This section overviews the ground based experiment which is a precursor of our microgravity experiment. Of course, some practical modifications related to layout and safety are necessary in preparation for a zero-g flight.

Overview

As shown in Figure 3, the experimental setup consists of a water vessel in which a single isolated cavity is produced, a high speed camera, flash lamps, and a laser with optical system to produce the cavity. The water vessel is made of plastic panels (Lexan). However for optimal optical quality, glass is the preferred material. The high speed CCD-camera used is a Photron Ultima APX, running at 87'600 frames/s. This camera films only a short interval (11 ms) covering the cavity life cycle (growth and collapse). Because of the rapid shutter speed (1/250'000) powerful flash lamps are needed to illuminate the sequence (Cordin Light Source Model 359). This imaging system has been tested in microgravity during the 8th student parabolic flight campaign and 42nd ESA parabolic flight campaign (Obreschkow et al. 2006a & 2006b).
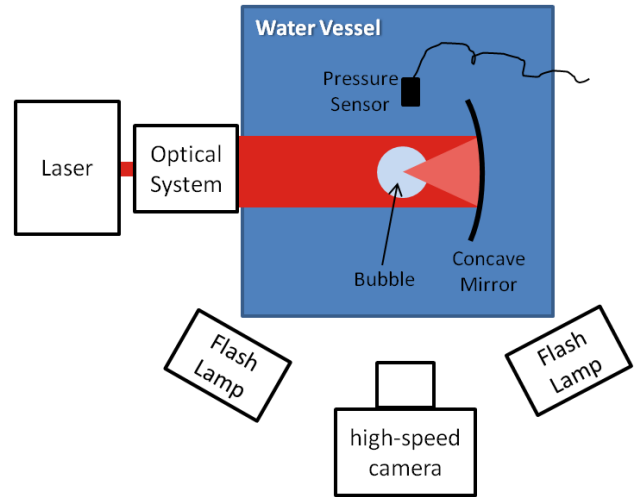

Figure 3 : Experimental setup

Figure 4 shows the experiment mounted on an optical board in the laboratory. Due to the large size and weight (>150kg) of the components necessary for the experiment (not all are visible on Figure 4), the experiment is particularly well suited for parabolic flights, as opposed to other microgravity possibilities. The experiment mounted on the airplane would be very similar, bar some minor modifications for safety and reliability.
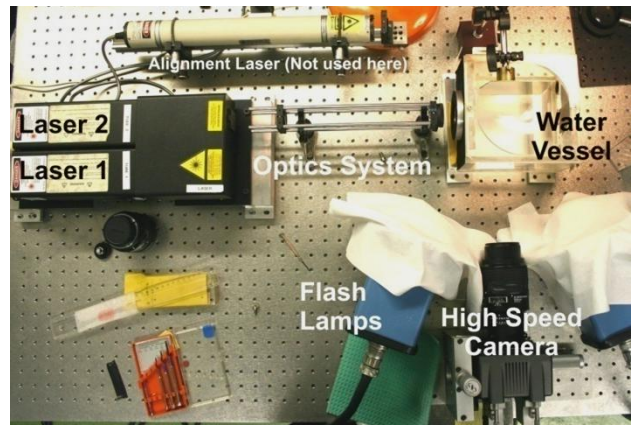

*Figure 4 : Experimental setup photo in lab*

Shockwave Detection

At the moment of cavity collapse, the emission of a high pressure front radiating from the collapse center has been observed. Similar shockwaves are observed at the moment of cavity generation. We can delimit the cavity lifetime by these two events. These shockwaves propagate radially at the speed of sound and it has been estimated that their peak pressure is of the order of the GPa. A thin pressure front of this order of magnitude can difficultly be measured directly, although the use of a hydrophone measuring the refractive index has been suggested (Akhatov et al. 2001).
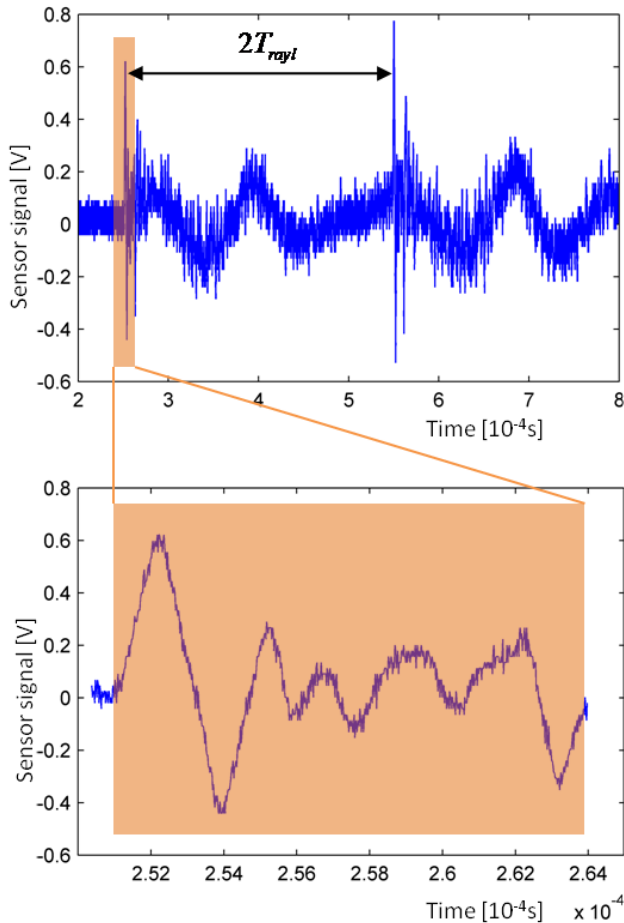
Figure 5a,b : Shockwave detection using pressure sensor

Piezo-electric pressure sensors react to changes in pressure; however the reaction time of a typical pressure sensor is slow compared to passage time of the shock front. Fortunately the shockwave excites the sensor and causes it to resonate, likely with a slight delay. Since only the time difference between peaks is of interest, this delay is unimportant for us. Figure 5 shows a typical such response. The time between the two pressure peaks is the double of the Raleigh collapse time. Once this value extracted, eq. (1.2) allows us to determine the bubble maximum radius. This radius corresponds precisely to the one measured directly with the high speed camera. This confirms the association of the pressure peaks with the shockwaves emitted at cavity generation and collapse, and validates their detection by our pressure sensor.

Signal processing was performed as described below in order to automate the process of finding the Rayleigh collapse time and improve consistency and accuracy.
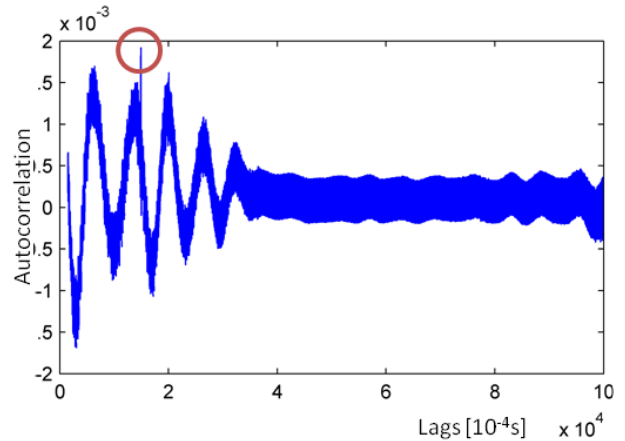
Figure 6 : Autocorrelation of the pressure sensor signal

After autocorrelation, certain harmonics are visible but do not "hide" the maximum value as visible on Figure 6. The value of the autocorrelation which occurs when the two peaks are superposed is visibly pronounced. The Rayleigh collapse time can be easily and consistently extracted.

Assuming the sensor responds linearly to the passage of this violent pressure front, the relative intensity between different shockwaves can be determined and compared. We define this intensity of the shockwave as the maximum value of the second peak (collapse shockwave).

After the passage of the shockwave, an interesting harmonic is visible (Figure 5a); however its interpretation is not clear. In the zoomed segment (Figure 5b), the resonant frequency of the sensor is well visible.

Laser Cavity Generator

Generating the cavity is the most delicate part of our experimental setup. Two standard methods for generating a single cavity are an electrical arc (using electrodes) or a laser beam. In the case of this investigation, the cavity must be very spherical and undisturbed, thus a laser is the preferred method for generating the cavity. The presence of electrodes would deform the cavity during collapse.

The cavity is generated using an Nd:YAG laser (New Wave Research Minilase III-15; 532nm, ~50mJ pulse in 6ns – 8MW) focused on a single point in the water vessel. An optical system is used to minimize aberration and approach a perfect focus. A poor focus is considered a bubble shape disturbance, therefore the optical system is a critical element to optimize and will comprise an important part of the following discussion.

It is thought that by increasing the angle of convergence (Figure 7) of the focused laser beam, the focus is better and so also the resulting cavity. An increased angle also decreases the region in which the energy density is high enough for plasma formation.
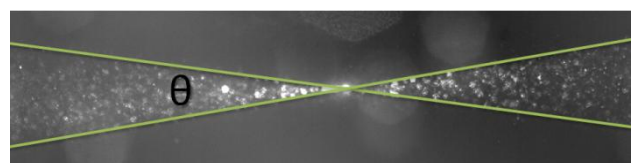
Figure 7 : Angle of convergence (laser visible, no cavity)

A Galilean type beam expander (Figure 8) was used to decrease aberrations and increase the convergence angle of the beam.
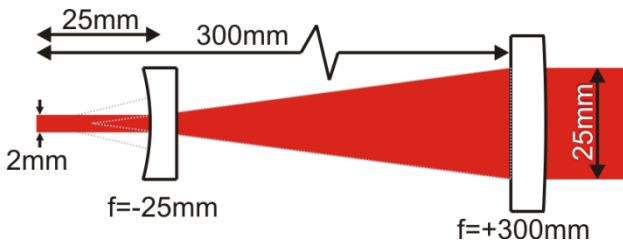

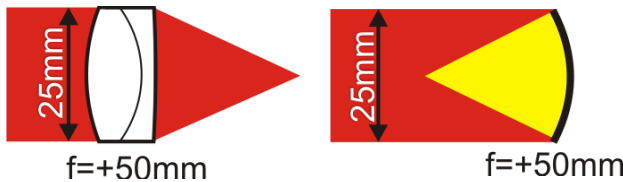*Figure 8 : Galilean beam expander, 12x expansion factor*

Figure 9 : Converging lens, Concave mirror

During adjustment and tuning, cavities were generated under different "focal" conditions. In particular, the expanded beam was focused using a converging lens and a concave parabolic mirror (Figure 9), and the two methods were compared. The initial bubble sphericity was observed, as was the size of the rebound bubbles. The visual sphericity of the bubbles and their consequent collapse and rebound was seen to be related to the shape of the initial plasma. Comparing two extreme but characteristic cases brings this to light (Figure 10a,b). It was observed that the cavities produced with the concave mirror were significantly more spherical than those produced with the converging lens.
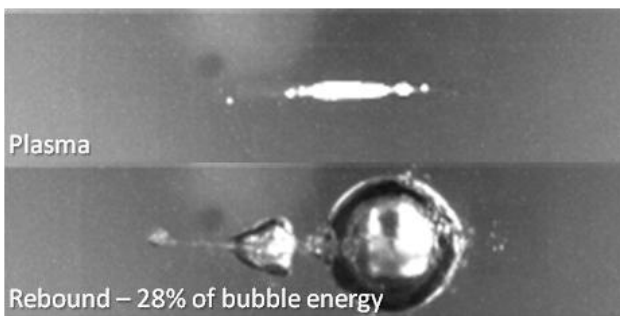

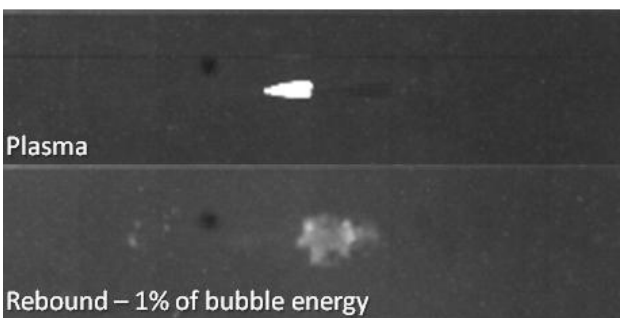*Figure 10a : Plasma and rebound using a converging lens*

Figure 10b: Plasma and rebound using a concave mirror

A quantitative picture of the influence of the geometry on the rebound bubble energy is given in Figure 11.
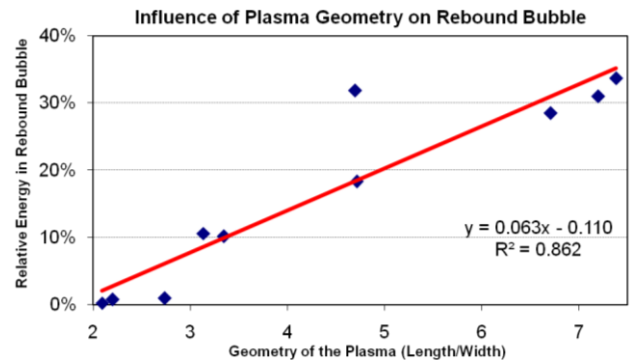

Figure 11 : Relative rebound energy as a function of plasma geometry (which is thought to cause bubble deformation)

This is not a rigorous examination of the nature of the plasma or the rebound bubble, but clearly the geometric shape of the plasma (quality of the laser focus) has a significant influence on how much energy is dissipated in the form of a rebound bubble. In the case of the concave mirror, the cavity is more spherical and it is thought that more energy is dissipated by other means (ex: shockwave).

Optical Improvements

The importance of beam focus led to the search of possible optical improvements. In reality, a beam is not homogenous but its energy distribution is Gaussian. Even after expansion, the most powerful part of the beam has a relatively low angle of convergence, since it is in the center of the converging beam. Additionally, before the beam reaches the mirror, this powerful peak passes through the area where the bubble will form, possibly heating the surrounding water and influencing the bubble's collapse.

A device was imagined and built to address these key issues. The "beam splitter" used was custom manufactured, since none appeared available on the market. As depicted in Figure 12 the input is an expanded laser beam which is reflected radially by a conical mirror. A second conical surface reflects the beam once again axially giving a "ring beam" output.

Figure 12 : Principle of "beam splitter"

The beam splitter was manufactured using standard machining techniques (e.g.: lathe to ~0.01mm precision) and then subsequently rectified (polished). The two mirrored surfaces were produced by electro-deposition of nickel.

Tests were performed by inserting this beam splitter between the beam expander and the concave mirror. The beam splitter functioned as expected. However, cavities could not yet be generated in this configuration. It is thought that the nickel coating does not sufficiently reflect the laser beam and too much of the beam is diffused. A plasma does not form and there is no cavity. We believe that a better mirror coating, using another technique would make the beam splitter function as desired.

Results and Discussion

In microgravity we will measure the different energy dissipation channels of a collapsing bubble in the absence of disturbing buoyancy forces. The goal is to investigate the dissipations mechanisms of a perfectly spherical bubble collapse.

In preparation for this microgravity experiment, we decided to vary the bubble sphericity indirectly, by changing the bubble size. While the bubble surface is proportional to r^2 (r=radius), the buoyancy force scales as r^3 according to the Archimedes principle. Thus the surface of smaller bubbles is less disturbed and hence more spherical than the surface of larger bubbles.

By varying the energy in the laser pulse, we plotted the relative energy dissipated by shockwaves (Figure 13) and by bubble rebound (Figure 14). Note that the units of Figure 13 are not normalized.
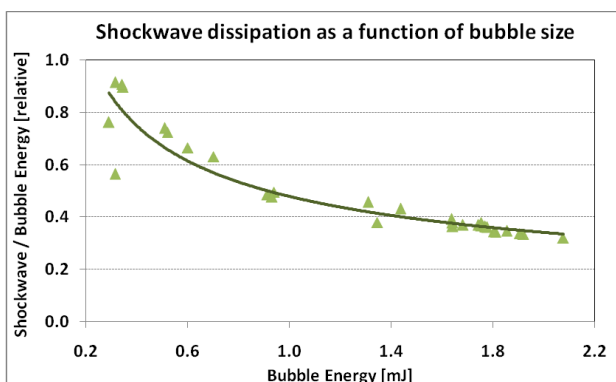

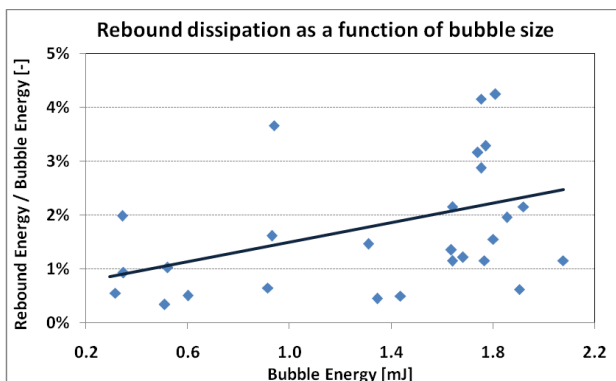Figure 13 : Effect of buoyancy forces on shockwave dissipation

Figure 14 : Effect of buoyancy forces on rebound dissipation

As bubble energy increases (size increases, sphericity decreases), the amount of energy dissipated in the form of a shockwave decreases, while energy dissipated in the form of a rebound bubble increases. It appears that the more a bubble is deformed the less is the importance of the shockwave. This is in accordance with the trend of deformed plasmas having larger rebound bubbles, as we saw in Figure 11. In microgravity the results of (Matula 2000) demonstrated increased sonoluminescence. In the same line, Benjamin and Ellis (Benjamin and Ellis 1966) demonstrated that large bubbles will deform due to the hydrostatic pressure field in water, influencing the cavity collapse and causing preferential microjet propagation.

All this evidence makes a clear prediction of the energy dissipation of a perfectly spherical bubble collapse achievable in microgravity: no liquid jets, relatively small rebound bubbles, very strong shockwaves, intensified sonoluminescence, and maybe even controversial cold fusion.

Conclusion

We have presented a future microgravity experiment and preliminary results on collapsing cavitation bubbles. If very small bubbles do in fact resemble conditions in microgravity, we expect small rebound bubbles and important dissipation through other mechanisms, such as discussed in the last paragraph of the preceding section. However, there may be significant differences difference between small (nearly spherical) bubbles produced on earth and perfectly spherical bubbles produced in microgravity.

Only results in microgravity (variation or absence of hydrostatic pressure field) can help establish a true cause and effect relationship between bubble sphericity and the energy dissipation mechanisms. Additionally, shockwave intensity in microgravity conditions would be measured for the first time. Significant insight will be given into the final stages of a nearly perfect spherical bubble collapse and the mechanisms of energy dissipation at the moment of collapse.

The proposed setup is quite general, and could equally well be adopted for other forthcoming cavitation studies in microgravity. Such research could give more insight into the possibility of so-called bubble cold fusion and other related phenomena.

Akhatov, I., O. Lindau, A. Topolnikov, R. Mettin, N. Vakhitova, and W. Lauterborn. "Collapse and rebound of a laser-induced cavitation bubble." *Physics of Fluids* 13, no. 10 (2001): 2805-2819.

Benjamin, T. B., and A. T. Ellis. "The collapse of cavitation bubbles and the pressure therby produced against solid boundaries." *Phil. Trans. R. Soc. Lon.* 260, no. 1110 (1966): 221-240.

Matula, T. J. "Single-bubble sonoluminescence in microgravity." *Ultrasonics* 38, no. 1-8 (2000): 559-565.

Obreschkow, D., P. Kobel, N. Dorsaz, A. de Bosset, and M. Farhat. "Microgravity experiment: The Fate of Confined Shockwaves." *IAC 2006*, (2006a).

Obreschkow, D., P. Kobel, N. Dorsaz, A. de Bosset, C. Nicollier, and M. Farhat. "Cavitation Bubble Collapse inside Liquid Drops in Microgravity." *Physical Review Letters 97, 094502*, (2006b).

Plesset, M. S. "The dynamics of cavitation bubbles." *J. Appl. Mech.* 16, no. 277 (1949).

Rayleigh, L. "On the pressure developed in a liquid during the collapse of a spherical cavity." *Philos. Mag.* 94, no. 34 (1917).